




Adsorption and diffusion of CO₂ and CH₄ in covalent organic frameworks: an MC/MD simulation study

Hongwei Zeng, Yu Liu & Honglai Liu


To cite this article: Hongwei Zeng, Yu Liu & Honglai Liu (2018) Adsorption and diffusion of CO₂ and CH₄ in covalent organic frameworks: an MC/MD simulation study, Molecular Simulation, 44:15, 1244-1251, DOI: [10.1080/08927022.2018.1481959](https://doi.org/10.1080/08927022.2018.1481959)

To link to this article: <https://doi.org/10.1080/08927022.2018.1481959>

 View supplementary material 

 Published online: 11 Jun 2018.

 Submit your article to this journal 

 Article views: 133

 View Crossmark data 



Adsorption and diffusion of CO₂ and CH₄ in covalent organic frameworks: an MC/MD simulation study

Hongwei Zeng^a, Yu Liu^a and Honglai Liu^b

^aState Key Laboratory of Chemical Engineering and School of Chemical Engineering, East China University of Science and Technology, Shanghai, People's Republic of China; ^bState Key Laboratory of Chemical Engineering and School of Chemistry & Molecular Engineering, East China University of Science and Technology, Shanghai, People's Republic of China

ABSTRACT

Covalent organic frameworks (COFs) are a promising gas separation material which have been developed recently. In this work, we have used grand canonical Monte Carlo (GCMC) and molecular dynamics (MD) simulations to investigate the adsorption and diffusion properties of CO₂ and CH₄ in five recent synthesised COF materials. We have also considered the properties of amino-modified COFs by adding –NH₂ group to the five COFs. The adsorption isotherm, adsorption/diffusion selectivity, self/transport diffusion coefficients have been examined and discussed. All of the five COFs exhibit promising adsorption selectivity which is higher than common nanoporous materials. An S-shaped adsorption isotherm can be found for CO₂ instead of CH₄ adsorption. The introduction of –NH₂ group is effective at low pressure region (<200 kPa). The diffusion coefficients are similar for TS-COFs but increase with the pore size for PI-COFs, and the diffusion coefficients seem less dependent on the –NH₂ groups.

ARTICLE HISTORY

Received 25 August 2017
Accepted 23 May 2018

KEYWORDS

Covalent organic frameworks; grand canonical Monte Carlo; molecular dynamics; adsorption; separation

1. Introduction

Developing high performance CO₂/CH₄ separation material is an important issue in energy and environmental field, which has attracted worldwide concern. In the past decades, various experimental and theoretical studies have been carried out to find promising CO₂/CH₄ separation materials. For example, in experimental field, Bastin et al. synthesised MOF-508b and tested its adsorption properties for CO₂/CH₄, CO₂/N₂ and CO₂/CH₄/N₂ mixtures by fixed-bed adsorption, respectively, and the selectivity is approximately 3–6 [1]. Hamon et al. examined the separation of CO₂/CH₄ in a breathing MOF, MIL-53(Cr), and the highest selectivity is reported to be 15 [2]. Shan et al. synthesised ACOF-1 based mixed-matrix membranes (MMMs) to separate CO₂ from CO₂/CH₄ mixture and found the 8 wt% ACOF-1@ Matrimid is the most favourable separation material, where the selectivity reaches 30–32 [3]. Venna and Carreon synthesised ZIF-8 membranes with thickness 5–9 μm to separate CO₂ from CO₂/CH₄, which show not only good equilibrium properties (adsorption selectivity 4–7) but also an excellent diffusion properties (permeance 2.4×10^{-5} mol/m²/s/Pa) [4]. In theoretical field, Babarao et al. studied the separation of CO₂ and CH₄ in silicalite, C₁₆₈ schwarzite and IRMOF-1 by GCMC simulation, respectively, and found that IRMOF-1 has the highest adsorption capacity but similar adsorption selectivity comparing to silicalite and C₁₆₈ schwarzite [5]. Krishna and van Baten screened out 12 zeolites for CO₂/CH₄ separation by GCMC simulation and MD simulation [6]. Liu et al. investigated the adsorption of CO₂ and CH₄ in ZIF-8 and Zn₂(BDC)₂(ted) with density functional theory (DFT) and GCMC simulation [7]. Bae et al.

investigated CO₂/CH₄ adsorption in a mixed-ligand metal-organic framework (MOF) Zn₂(NDC)₂(DPNI) by GCMC simulation, where the selectivity was reported on order of 30 [8].

Covalent organic frameworks (COFs) are a class of novel crystalline porous polymers that consist of light elements (such as C, H, O, N, B and Si) and structured by their strong covalent bonds (such as B–O, C–N, B–N and B–O–Si) [9,10]. Since its first being synthesised by Yaghi et al. in 2005 [9], COFs have revealed itself as a promising material in gas adsorption and storage [11–13] due to its enormous surface area, porosity and high stability. For example, Furukawa and Yaghi examined the storage of H₂, CH₄ and CO₂ in seven COFs, and found COF-102 to be the best adsorption material [14]. Mendozacortés et al. investigated methane adsorption in nine COFs including 2D and 3D structures by GCMC with force field developed from quantum mechanics, and found COF-1 to be the favourable CH₄ storage material, whose uptake exceeds the U.S. Department of Energy (DOE) target [15]. Babarao and Jiang [16] have studied CO₂ storage in eight COFs including 3D, 2D and 1D structures through Gibbs ensemble Monte Carlo (GEMC) simulation. By performing first-principle calculations and grand canonical Monte Carlo (GCMC) simulations, Lan et al. found that doping Li in COFs can largely enhance its uptake of CO₂ [17]. Choi et al. designed 2D COF-05, 3D COF-05 (ctn) and 3D COF-05 (bor) by combining *ab initio* calculations and force field calculations and found these COFs can provide an reversible CO₂ uptake capacity at room temperature [18].

In this work, we will use GCMC and MD simulations to study the thermodynamic and kinetic properties of CO₂ and

CH₄ adsorption in five recent synthesised COF materials and evaluate their prospects in CO₂ capture. In the following section, we will introduce the modelling and simulation details of the five materials; the numerical results will be exhibited and discussed in Section 3; finally, conclusions will be drawn in Section 4.

2. Modelling and simulations

Figure 1 shows the five COFs considered in this work, which are named by TS-COF-1, TS-COF-2, PI-COF-1, PI-COF-2 and PI-COF-3, respectively. The COFs are composed of six-membered ring with pore size ranges from 19 to 53 Å [19,20], where the TS-COFs are triazine functionalised and PI-COFs are pyromellitic dianhydride (PMDA) functionalised. We used molecular mechanics (MM) method to optimise the structure of the COFs before the GCMC and MD simulations, which will be assumed to be rigid in the GCMC and MD simulations. The MM optimisation is performed in the Forcite module of the Material Studio software, where the atom–atom interaction is modelled by the COMPASSII force field. The electrostatic interaction is calculated by the Ewald summation method with an accuracy 1×10^{-5} kcal/mol. The long range tail of the Lennard–Jones (LJ) potential is truncated at 15 Å, where the discontinuity of the interacting potential at the truncation point is smoothed by the cubic spline method with a spline width 1 Å and a buffer width 0.5 Å. The information of the optimised calculation box and the pore diameter are shown in Table 1.

Table 1. Detailed structural information of the five COFs.

COF	TS-COF-1	TS-COF-2	PI-COF-1	PI-COF-2	PI-COF-3
Sim. density (g cm ⁻³)	0.54	0.79	0.58	0.50	0.35
Exp. density (g cm ⁻³)			0.64	0.55	0.39
Sim. pore size (Å)	36	19	33	37	53
Exp. pore size (Å)	33	15	33	37	53
Box size x (Å ³)	36×36×35	19×19×35	33×33×34	37×37×34	53×53×52

GCMC simulation was used to study the thermodynamic properties of CH₄ and CO₂ in COFs. The sorption module in the Material Studio software was used to implement the computation. 1×10^7 microstates were generated in total by the Metropolis sampling, where the first 1×10^6 microstates were used for equilibrium (Figure S1 in the supporting information), while the other 9×10^6 microstates were used for statistics. The relationship between fugacity and pressure for the bulk phase is calculated by the corresponding state theory. The adsorption selectivity for component A relative to component B is defined as

$$S_{\text{sorp}} = \left(\frac{x_A}{x_B} \right) \left(\frac{y_B}{y_A} \right), \quad (1)$$

where x_A and x_B are the mole fractions of components A and B in the absorbed phase while y_A and y_B are the corresponding mole fractions in the bulk phase, respectively [5,8,21–23].

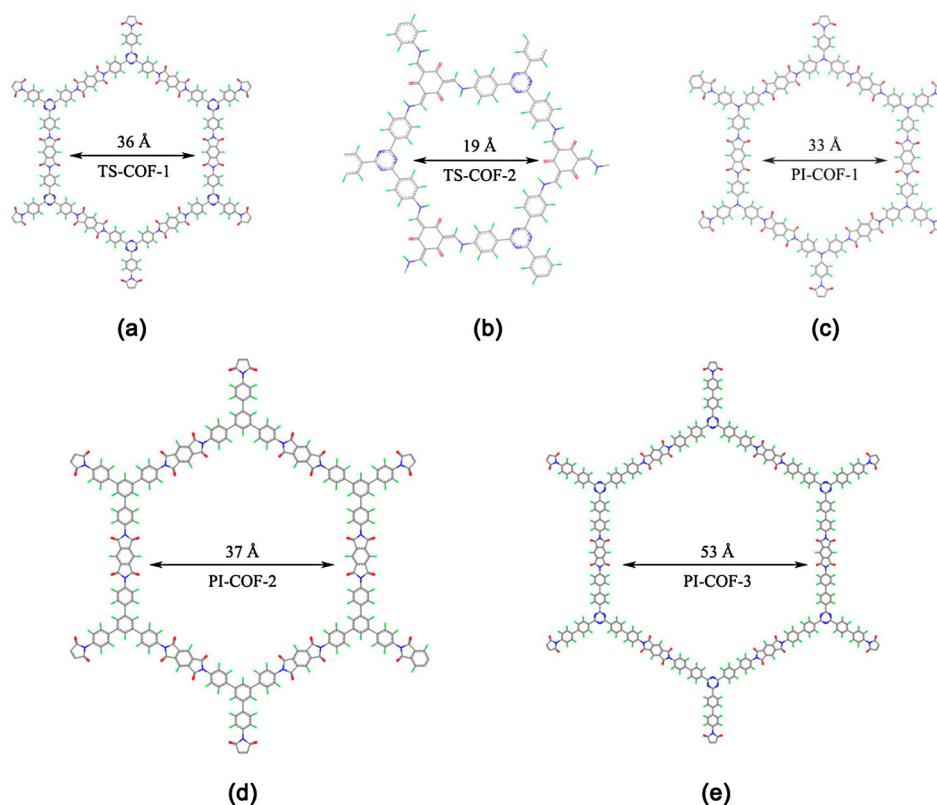


Figure 1. (Colour online) (a) TS-COF-1 with pore size of 36 Å; (b) TS-COF-2 with pore size of 19 Å; (c) PI-COF-1 with pore size of 33 Å; (d) PI-COF-2 with pore size of 37 Å; (e) PI-COF-3 with pore size of 53 Å (C, grey; H, green; N, blue; O, red).

The kinetic properties were represented by two diffusion coefficients: one is the self-diffusivity D_s and the other is the transport diffusivity D_t . D_s was obtained from the mean square displacement (MSD) of individual molecule, which is calculated via the Einstein equation [24,25]:

$$D_s = \lim_{t \rightarrow \infty} \frac{1}{6Nt} \left\langle \sum_{i=1}^N \left| \vec{r}_i(t) - \vec{r}_i(0) \right|^2 \right\rangle, \quad (2)$$

where N is the number of adsorbate molecule, t is the time, $\vec{r}_i(t)$ is the position of molecule i at time t and the brackets represents the ensemble average. D_t is defined by Fick's law of diffusion [26,27]:

$$\vec{J} = -D_t \nabla c, \quad (3)$$

where \vec{J} is the flux, ∇c is the gradient of the concentration, which can also be calculated by [25–28]

$$D_t = D_c \left(\frac{\partial \ln f}{\partial \ln c} \right)_T, \quad (4)$$

where f is the fugacity of the bulk phase, c is the concentration of the adsorbed phase and D_c is the corrected diffusivity, which can be calculated by [26,28]

$$D_c = \lim_{t \rightarrow \infty} \frac{1}{6Nt} \left\langle \left| \sum_{i=1}^N [\vec{r}_i(t) - \vec{r}_i(0)] \right|^2 \right\rangle. \quad (5)$$

We used equilibrium molecular dynamics (EMD) simulation to calculate D_s and D_c for CH_4 and CO_2 in COFs, respectively, while D_t is calculated by Equations (4) and (5), where the relationship between f and c was generated by the GCMC simulation and the partial derivative is obtained by the slope of the adsorption isotherm ($\ln f - \ln c$ plot) in Figures S4–S13 in the supporting information (SI). The EMD simulation was implemented in the Forcite module. 10 independent simulations were performed for each system with NVT ensemble. The total simulation time was 2 ns with a time step 1 fs, where the first 1 ns was used for equilibrium and the other 1 ns is used for statistics.

The diffusion selectivity is defined as the ratio of the self-diffusivities of components A and B [6,22]:

$$S_{\text{diff}} = \frac{D_{s,A}}{D_{s,B}}. \quad (6)$$

As the focus of this work is on the room temperature region, we have used the ideal adsorbed solution theory (IAST) to calculate the adsorption/diffusion selectivity, whose accuracy has been well examined by the previous literatures [8,22,29].

3. Results and discussion

First, the accuracy of the modelling has been examined by comparing to experimental data and previous simulations [5]. Figure 2 shows the adsorption isotherms of CO_2 and CH_4 in IRMOF-1 at 300 K. For CH_4 , our simulation nicely reproduces the experimental data and accord with Babarao et al. simulation. For CO_2 , comparing to experimental data, our simulation captures the essentials of the adsorption isotherm but

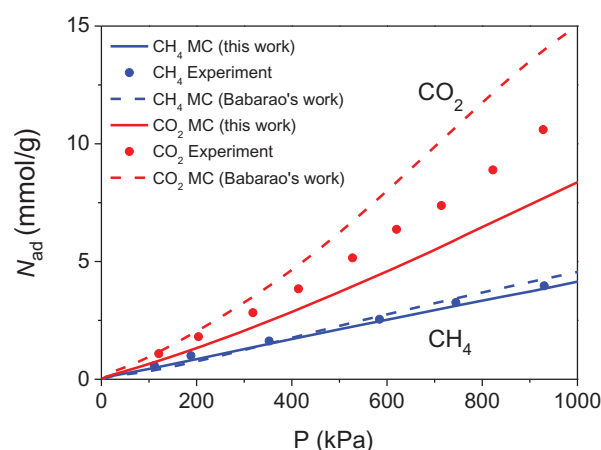


Figure 2. (Colour online) Adsorption isotherms of CO_2 and CH_4 in IRMOF-1 at 300 K. Experimental data and Babarao et al. simulation come from Ref. [5].

slightly lower estimate the uptake quantitatively, which is in contrast to Babarao et al. simulation. The good agreement between our model and the experimental data shows the accuracy of the modelling, and in the following of this article, we will use the model to predict CO_2 and CH_4 adsorption/diffusion in COFs.

Figure 3(a,b) shows the CO_2 and CH_4 adsorption isotherms for the five COFs at 298 K, respectively. The five COFs exhibit similar adsorption isotherm for CH_4 in contrast to CO_2 , and the uptake of CO_2 is higher than CH_4 by 1 order of magnitude. There is a well-known electric quadrupole for CO_2 molecule, which may result in a strong attraction between CO_2 and the COFs; in contrast, CH_4 is more like a spherical molecule, which results in a weak attraction. In the low pressure region (<200 kPa), as there are plenty of free volume in the adsorbent, the adsorption is dominated by the adsorbent–adsorbate attraction, and the uptake of CO_2 increases sharper than CH_4 . Due to the low attraction of CH_4 , the energy/free energy of the CH_4 –COF system is dominated by its ideal gas term which resulted in similar and near-ideal adsorption isotherms (Figure 3b). When the adsorption approaches saturation, the adsorbate–adsorbate repulsion is the dominating factor and the saturated uptake is proportional to the void fraction of the adsorbent. This is consistent with Figure 3(a), where the order of the saturated uptake is given by PI-COF-3 > PI-COF-2 > TS-COF-1 > PI-COF-1 > TS-COF-2. In Figure 3(a), PI-COF-3 exhibited an obvious S-shaped adsorption isotherm instead of a Langmuir type, which implies a multilayer adsorption. This can be further exhibited by their density profiles as shown in Figure 3(c,d). Due to the strong attraction and the orientation dependence, it is possible for CO_2 instead of CH_4 to form multilayered structures. Figure 3(e) compares the adsorption selectivity (CO_2/CH_4) of the five COFs. The peak of the curves denotes the favourable adsorption selectivity, where the highest selectivity reaches 24. The formation of the peaks can be understood as follows: as reported in the literature [30], at 298 K, entropy effect mainly comes from the ideal term, which is similar for CH_4 and CO_2 . Therefore, the difference between these fluids should be understood by their enthalpic effect (interaction energies). At low pressure,

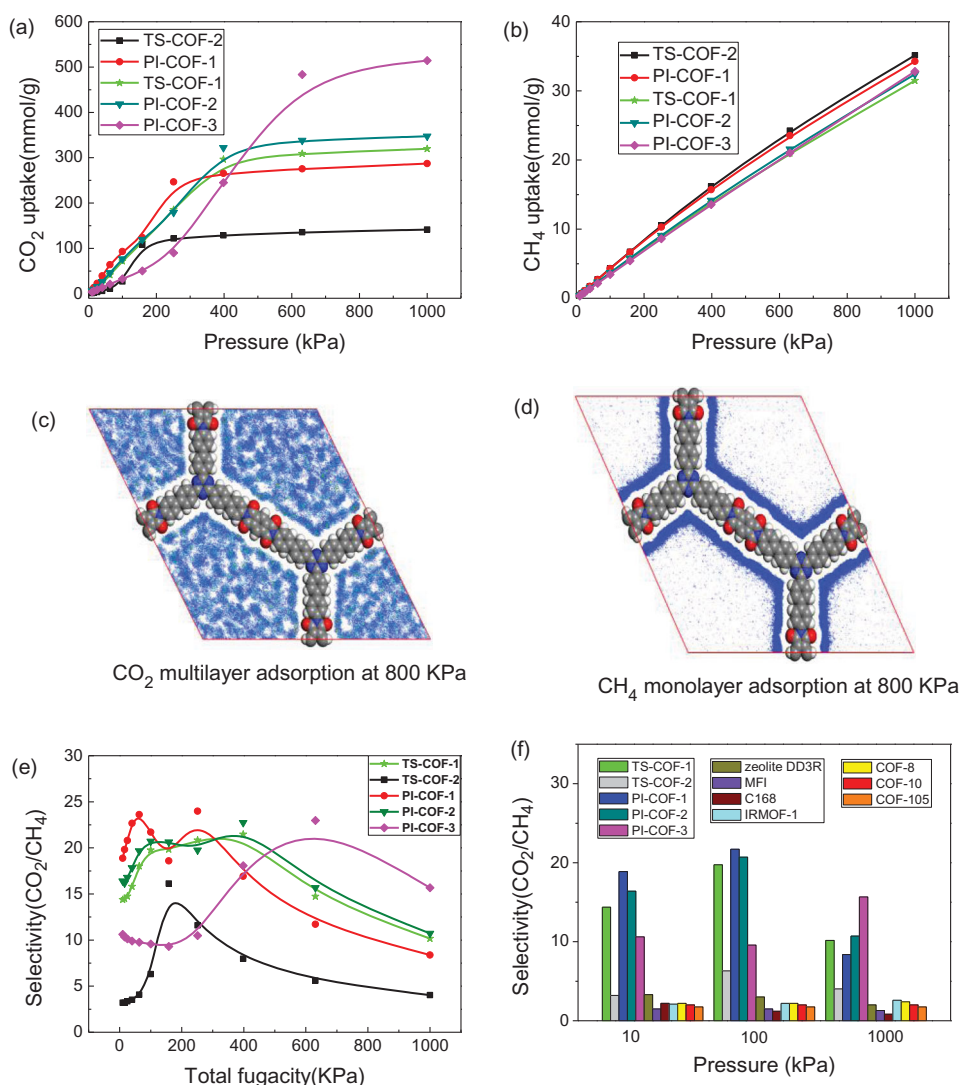


Figure 3. (Colour online) Adsorption isotherm of (a) CO_2 and (b) CH_4 in the five COFs, respectively; density distribution of (c) CO_2 and (d) CH_4 adsorption at 800 kPa (blue point denotes the mass centre of the adsorbate in the samplings). (e) Adsorption selectivity of the five COFs; (f) comparison for adsorption selectivity of the five COFs, DD3R, MFI, C₁₆₈, IRMOF-1, COF-8, COF-10 and COF-105. The curves are the B-Spline interpolation of the point servers as the guides to the eye.

inserting adsorbate molecule will decrease the free energy for CO_2 due to its strong attraction but will increase the free energy for CH_4 due to its weak attraction and the competition of free volume. Therefore, the selectivity for $\text{CO}_2/$

CH_4 will increase at low pressure, and the decreasing trend at high pressure (>600 kPa) due to the saturation of CO_2 , which finally resulted in a peak of the selectivity isotherm. Comparing the five COFs with other porous materials such

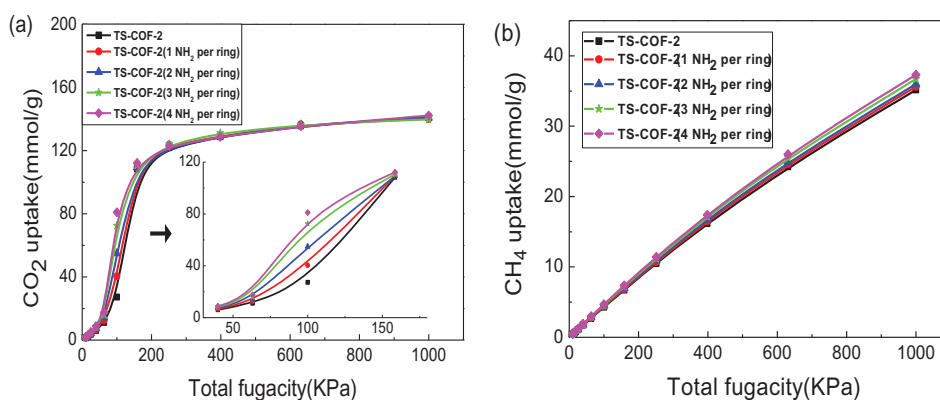


Figure 4. (Colour online) Adsorption isotherm for (a) CO_2 and (b) CH_4 in $-\text{NH}_2$ modified TS-COF-2, respectively.

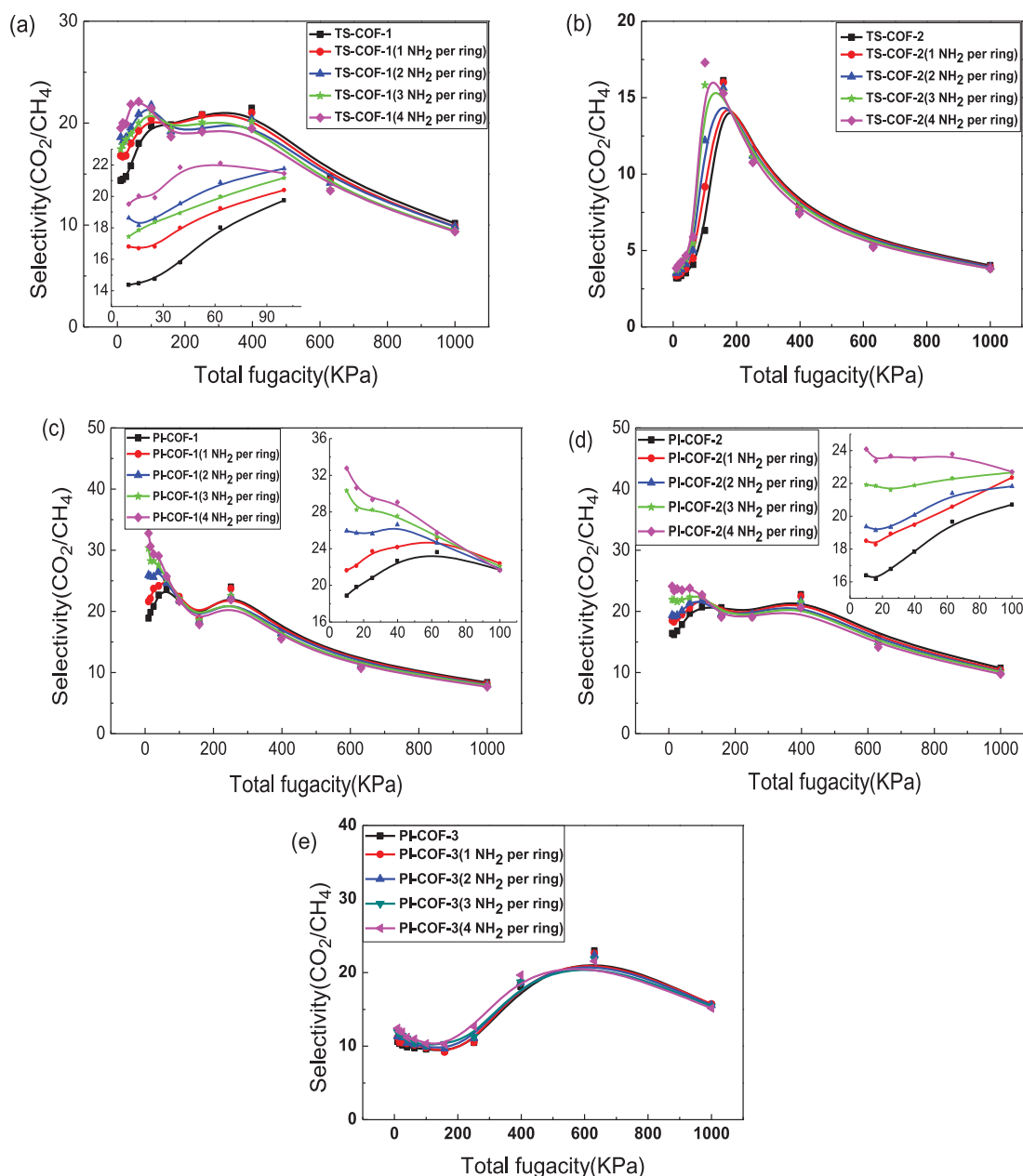


Figure 5. (Colour online) Adsorption selectivity (CO_2/CH_4) of (a) TS-COF-1, (b) TS-COF-2, (c) PI-COF-1, (d) PI-COF-2 and (e) PI-COF-3.

as DD3R, MFI, C_{168} , IRMOF-1, COF-8, COF-10 and COF-105 [5,22,31], as shown in Figure 3(f), it seems the five COFs studied in this work are more promising for CO_2/CH_4 separation, and PI-COF-1 and PI-COF-3 seem the most favourable material for low and high pressure, respectively.

Furthermore, we consider the adsorption properties of amino-modified COFs by binding $-\text{NH}_2$ group to the COFs. Figure 4 shows the influence of the $-\text{NH}_2$ group on the adsorption isotherm (the results for other COFs are provided in the supporting information). On one hand, the introducing of $-\text{NH}_2$ could strengthen the adsorption of CO_2 and CH_4 at low and medium pressure (200–600 kPa) as $-\text{NH}_2$ could provide extra adsorbent–adsorbate attraction and the surface area. On the other hand, $-\text{NH}_2$ may slightly decrease the saturated uptake as the introducing of functional

group could decrease the void fraction. Therefore, to improve the adsorption of CO_2 and CH_4 , $-\text{NH}_2$ group is effective only at low and medium pressure regions. According to Figure 4, Figures S2 and S3 (supporting information), in the standard condition, adding one $-\text{NH}_2$ per COFs ring will result in a 0.11–1.35 mmol/g and a 0.01 mmol/g increment on the uptakes for CO_2 and CH_4 , respectively, i.e. one $-\text{NH}_2$ group will adsorb extra 0.2–2.8 CO_2 molecules or 0.02 CH_4 molecules. TS-COF-2 resulted in a relatively larger increment of CO_2 uptake (2.8 CO_2 per $-\text{NH}_2$), this is because the pore size of TS-COF-2 is the smallest, grafting an $-\text{NH}_2$ will increase the specific surface area more dramatically. Figure 5 shows the influence of amino group on adsorption selectivity. Again, the $-\text{NH}_2$ is effective only at low and medium pressure regions for the five COFs. The increments of selectivity on low pressure limit ranging from 5 to 20 depend on

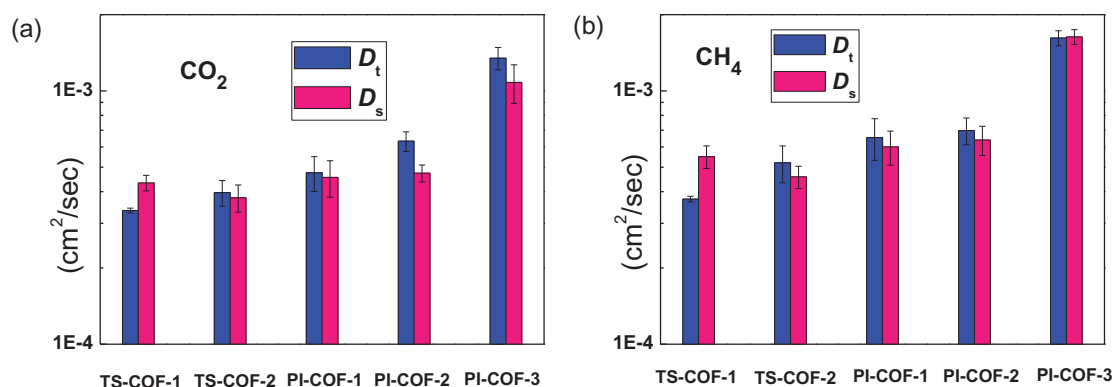


Figure 6. (Colour online) D_s and D_t of (a) CO₂ and (b) CH₄.

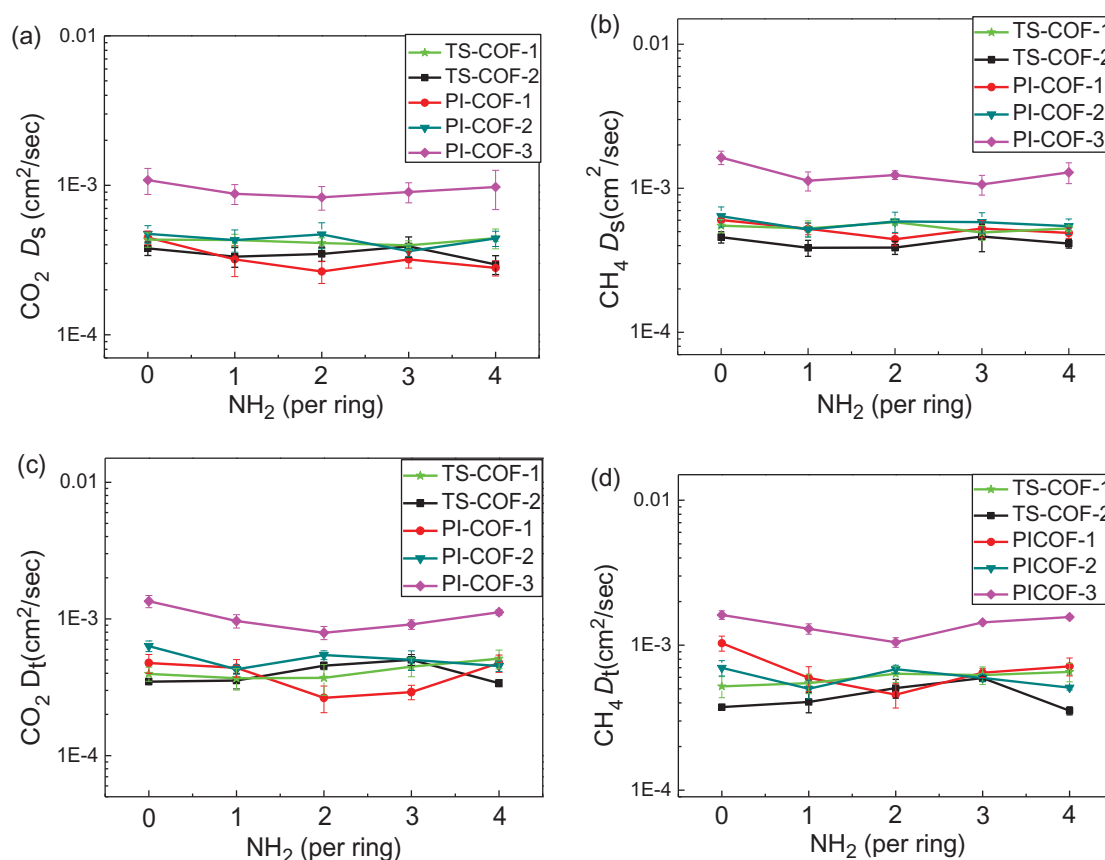


Figure 7. (Colour online) D_s of (a) CO₂ and (b) CH₄; D_t of (c) CO₂ and (d) CH₄.

the structure of the COFs, and it seems the increments are more obvious for COFs with smaller pore size.

Beside thermodynamics, the kinetic property is another important issue for porous materials. Figure 6 shows the self and transport diffusivities of the five COFs without modification. Although the definition of D_s and D_t is totally different, their numerical values are similar for the five COFs. The diffusion coefficients for the TS-COFs are similar, but increase with the pore size for PI-COFs. It seems the correlation between diffusion coefficient and pore size is valid only when pore size is larger than 30 Å; for smaller pores, the diffusion may

more depend on the detailed geometry and the charge distribution of the material. The diffusion properties for CO₂ and CH₄ are similar, which imply the quadrupole of CO₂ plays a less important role in diffusion.

Figures 7 and 8 show the influence of the -NH₂ groups on the diffusivity and diffusion selectivity. It seems the introduction of -NH₂ does not affect the diffusivities dramatically. The diffusion selectivity is approximately 0.5–1, which is much lower than that of the adsorption selectivity. Therefore, to separate CO₂/CH₄ in 2D COFs, one may more focus on their thermodynamic properties.

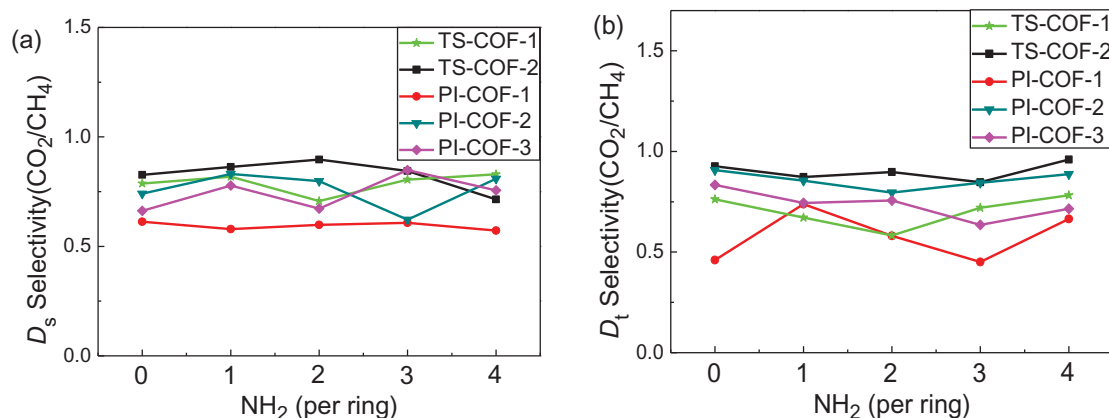


Figure 8. (Colour online) Diffusion selectivity (CO₂/CH₄) of the five COFs: (a) D_s and (b) D_t .

4. Conclusion

We have studied the adsorption and diffusion properties of CO₂ and CH₄ in five recent synthesised COF materials by the GCMC and EMD simulations. The favourable adsorption selectivity of the five COFs ranges from 16 to 24, which is higher than conventional nanoporous material, while the diffusion selectivity ranges from 0.5 to 1. PI-COF1 and PI-COF3 seem to be the best CO₂/CH₄ separation material in the five COFs for low and high pressures, respectively. An S-shaped adsorption isotherm has been observed for CO₂ adsorption, which implies a multilayer adsorption. The -NH₂ modified COFs exhibit higher uptakes and selectivity at low pressure region. The diffusion coefficients increase with pore size when pore diameter is larger than 30 Å. The diffusion properties for CO₂ and CH₄ are similar, which imply the quadrupole of CO₂ is less important for diffusion, and the -NH₂ group does not affect the diffusion coefficients significantly.

Disclosure statement

No potential conflict of interest was reported by the authors.

Funding

This work was supported by National Natural Science Foundation of China: [Grant Numbers 21506051, 21776070, 91334203]; Shanghai Pujiang Program: [Grant Number 15PJ1401400]; National Natural Science Foundation of China for Innovative Research Groups: [Grant Number 51621002]; National Basic Research Program of China: [Grant Number 2013CB733501]; Open Project of the State Key Laboratory of Chemical Engineering: [Grant Number SKL-Che-15C05]; 111 Project of China: [Grant Number B08021].

References

- [1] Bastin L, B rcia PS, Hurtado EJ, et al. A microporous metal–organic framework for separation of CO₂/N₂ and CO₂/CH₄ by fixed-bed adsorption. *J Phys Chem C*. **2008**;112(5):1575–1581.
- [2] Hamon L, Llewellyn PL, Devic T, et al. Co-adsorption and separation of CO₂–CH₄ mixtures in the highly flexible MIL-53 (Cr) MOF. *J Am Chem Soc*. **2009**;131(47):17490–17499.
- [3] Shan M, Seoane B, Rozhko E, et al. Azine-linked covalent organic framework (COF)-based mixed-matrix membranes for CO₂/CH₄ separation. *Chem Eur J*. **2016**;22(41):14467–14470.
- [4] Venna SR, Carreon MA. Highly permeable zeolite imidazolate framework-8 membranes for CO₂/CH₄ separation. *J Am Chem Soc*. **2010**;132(1):76–78.
- [5] Babarao R, Hu Z, Jiang J. Storage and separation of CO₂ and CH₄ in silicalite, C168 schwarzite, and IRMOF-1: a comparative study from Monte Carlo simulation. *Langmuir*. **2007**;23:659–666.
- [6] Krishna R, van Baten JM. Using molecular simulations for screening of zeolites for separation of CO₂/CH₄ mixtures. *Chem Eng J*. **2007**;133(1–3):121–131.
- [7] Liu Y, Liu H, Hu Y, et al. Density functional theory for adsorption of gas mixtures in metal–organic frameworks. *J Phys Chem B*. **2010**;114(8):2820–2827.
- [8] Bae Y-S, Mulfort KL, Frost H, et al. Separation of CO₂ from CH₄ using mixed-ligand metal–organic frameworks. *Langmuir*. **2008**;24(16):8592–8598.
- [9] Cote AP, Benin AI, Ockwig NW, et al. Porous, crystalline, covalent organic frameworks. *Science*. **2005**;310(5751):1166–1170.
- [10] Waller PJ, Gandara F, Yaghi OM. Chemistry of covalent organic frameworks. *Acc Chem Res*. **2015**;48(12):3053–3063.
- [11] Feng X, Ding X, Jiang D. Covalent organic frameworks. *Chem Soc Rev*. **2012**;41(18):6010–6022.
- [12] Ding SY, Wang W. Covalent organic frameworks (COFs): from design to applications. *Chem Soc Rev*. **2013**;42(2):548–568.
- [13] D  az U, Corma A. Ordered covalent organic frameworks, COFs and PAFs from preparation to application. *Coord Chem Rev*. **2016**;311:85–124.
- [14] Furukawa H, Yaghi OM. Storage of hydrogen, methane, and carbon dioxide in highly porous covalent organic frameworks for clean energy applications. *J Am Chem Soc*. **2009**;131(25):8875–8883.
- [15] Mendozacort  s JL, Sang SH, Furukawa H, et al. Adsorption mechanism and uptake of methane in covalent organic frameworks: theory and experiment. *J Phys Chem A*. **2010**;114(40):10824–10833.
- [16] Babarao R, Jiang J. Exceptionally high CO₂ storage in covalent-organic frameworks: atomistic simulation study. *Energy Environ Sci*. **2008**;1(1):139.
- [17] Lan J, Cao D, Wang W, et al. Doping of alkali, alkaline-earth, and transition metals in covalent-organic frameworks for enhancing CO₂ capture by first-principles calculations and molecular simulations. *ACS Nano*. **2010**;4(7):4225–4237.
- [18] Choi YJ, Choi JH, Choi KM, et al. Covalent organic frameworks for extremely high reversible CO₂ uptake capacity: a theoretical approach. *J Mater Chem*. **2011**;21(4):1073–1078.
- [19] Fang Q, Zhuang Z, Gu S, et al. Designed synthesis of large-pore crystalline polyimide covalent organic frameworks. *Nat Commun*. **2014**;5:1166.
- [20] Zhu X, An S, Liu Y, et al. Efficient removal of organic dye pollutants using covalent organic frameworks. *AIChE J*. **2017**. DOI:10.1002/aic.15699.
- [21] Liu Y, Liu D, Yang Q, et al. Comparative study of separation performance of COFs and MOFs for CH₄/CO₂/H₂ mixtures. *Ind Eng Chem Res*. **2010**;49(6):2902–2906.

- [22] Keskin S. Adsorption, diffusion, and separation of CH₄/H₂ mixtures in covalent organic frameworks: molecular simulations and theoretical predictions. *J Phys Chem C*. **2012**;116(2):1772–1779.
- [23] Vicent-Luna JM, Luna-Triguero A, Calero S. Storage and separation of carbon dioxide and methane in hydrated covalent organic frameworks. *J Phys Chem C*. **2016**;120(41):23756–23762.
- [24] Sanborn MJ, Snurr RQ. Diffusion of binary mixtures of CF₄ and *n*-alkanes in faujasite. *Sep Purif Technol*. **2000**;20(1):1–13.
- [25] Salles F, Jobic H, Devic T, et al. Self and transport diffusivity of CO₂ in the metal–organic framework MIL-47 (v) explored by quasi-elastic neutron scattering experiments and molecular dynamics simulations. *ACS Nano*. **2010**;4(1):143–152.
- [26] Ackerman DM, Skoulidas AI, Sholl DS, et al. Diffusivities of Ar and Ne in carbon nanotubes. *Mol Simul*. **2003**;29(10–11):677–684.
- [27] Skoulidas AI, Sholl DS. Self-diffusion and transport diffusion of light gases in metal–organic framework materials assessed using molecular dynamics simulations. *J Phys Chem B*. **2005**;109(33):15760–15768.
- [28] Skoulidas AI, Sholl DS. Molecular dynamics simulations of self-diffusivities, corrected diffusivities, and transport diffusivities of light gases in four silica zeolites to assess influences of pore shape and connectivity. *J Phys Chem A*. **2003**;107(47):10132–10141.
- [29] Keskin S, Liu J, Johnson JK, et al. Testing the accuracy of correlations for multicomponent mass transport of adsorbed gases in metal–organic frameworks: diffusion of H₂/CH₄ mixtures in CuBTC. *Langmuir*. **2008**;24(15):8254–8261.
- [30] Liu Y, Guo F, Hu J, et al. Entropy prediction for H₂ adsorption in metal–organic frameworks. *Phys Chem Chem Phys*. **2016**;18(34):23998.
- [31] Himeno S, Tomita T, Suzuki K, et al. Characterization and selectivity for methane and carbon dioxide adsorption on the all-silica DD3R zeolite. *Micropor Mesopor Mater*. **2007**;98(1–3):62–69.